Effect of Oxide Ion Distribution on Uranium Structure in Highly U-Doped $RE_2Hf_2O_7$ (RE = La and Gd) Nanoparticles

Yuming Wang,[a] *Pragathi Darapaneni,*[a] *Tochukwu Ofoegbuna,*[a] *Santosh K. Gupta,*[b] *Orhan Kizilkaya,*[c] *Yuanbing Mao,*[*,d] *and James A. Dorman,*[*,a]

[a] Cain Department of Chemical Engineering, Louisiana State University, Baton Rouge, Louisiana 70803, United States

[b] Radiochemistry Division, Bhabha Atomic Research Centre, Trombay, Mumbai 400085, India

[c] Center for Advanced Microstructures and Devices, Louisiana State University, Baton Rouge, Louisiana 70806, United States

[d] Department of Chemistry, Illinois Institute of Technology, Chicago, Illinois 60616, United States

ABSTRACT

Rare-earth based $A_2B_2O_7$ compounds have been considered as potential host materials for nuclear waste due to their exceptional chemical, physical, capability of accommodating high concentration of actinides at both A- and B-sites, negligible leaching, tendency to form antisite defects, and radiation stabilities. In this work, $La_2Hf_2O_7$ (LHO) and $Gd_2Hf_2O_7$ (GHO) nanoparticles (NPs) were chosen as the RE-based hafnates to study the structural changes and the formation of different U molecular structures upon doping (or alloying) at high concentration (up to 30 mol%) using a combined co-precipitation and molten-salt synthesis. These compounds form similar crystal structures, i.e. ordered pyrochlore (LHO) and disordered fluorite (GHO), but are expected to show different phase transformations at high U doping concentration. X-ray diffraction (XRD) and Rietveld refinement results show that the LHO:U NPs have high structural stability whereas the GHO:U NPs exhibit highly disordered structure at high U concentration. Alternatively, the vibrational spectra show an increasingly random oxygen distribution with U doping, driving the LHO:U NPs to the disordered fluorite phase. X-ray spectroscopy indicates that U is stabilized as different U^{6+} species in both LHO and GHO hosts, resulting in the formation of oxygen vacancies stemming from the U local coordination and different phase transformation. Interestingly, the disordered fluorite phase has been reported to have increased radiation tolerance, suggesting multiple benefits associated with the LHO host. These results demonstrate the importance of the structural and chemical effect of actinide dopants on similar host matrices which are important for the development of RE-based hafnates for nuclear waste hosts, sensors, thermal barrier coatings, and scintillator applications.

Keywords: Scintillators; Uranium; Nanoparticles; Radiation Stability; Phase Transitions

1. Introduction

The global challenge in the current nuclear technology is the management of radioactive waste after the spent nuclear fuels are reprocessed.[1] Multiple materials for high level waste (HLW) forms have been studied since 1950s, with investigations in borosilicate-,[2-3] phosphate-,[4] and nepheline-syenite-based glasses,[3] various polyphase ceramics,[5-6] bituminous, and concrete materials[7] due to their stability for long-time storage of nuclear waste. Among these different types of waste forms, borosilicate glasses have been widely used as host matrices to immobilize HLW for more than 25 years.[8] Unfortunately, borosilicate glass waste form tends to devitrify in the presence of water and steam due to the high temperature (300 °C in salt or 400 °C in other rocks) and pressure environment, resulting in damages to the glass container after burial in geological repositories.[8] Moreover, the high possibility of devitrification in these conditions increases the leachability of few highly dangerous species such as cesium and actinides.[6]

To overcome these devitrification issues, $A_2B_2O_7$ compounds have been used as a replacement of borosilicate glasses in the disposition and transmutation of long-lived isotopes, such as uranium, plutonium, neptunium, americium, and curium generated from nuclear power and weapons programs.[9-10] For most materials, irradiation creates atomic-scale defects in the host crystal, which accumulate with time and leads to material failure (i.e. amorphization or microcracking). However, when $A_2B_2O_7$ pyrochlore structures are exposed to radiation, two atomistic defects, cation antisite $(0 \rightarrow A_B + B_A)$ and anion Frenkel pairs $(0 \rightarrow V_O + O_i)$, are created.[11] These defects are responsible for the pyrochlore to fluorite order-disorder phase transformation, which contributes to maintaining the crystallinity of the host material.[11-12] Among these compounds, RE-based hafnates $RE_2Hf_2O_7$ have been studied in the past decade as potential host materials for HLW[13] due to their outstanding properties such as low thermal conductivity,[14] high melting point,[15] chemical and thermal stability.[16-17] Of the two possible crystal structures (ordered pyrochlore and defect fluorite), the defect fluorite structure is more favorable when the ratio of the A and B cation radii is less than 1.46 with oxygen vacancies randomly distributed on the anion sites. On the other hand, ordered pyrochlore structure is stable when this ratio is greater than 1.46 with 8-fold oxygen coordinated RE^{3+} site and 6-fold oxygen coordinated Hf^{4+} site.[18-21] While ordered pyrochlore structure can have the dopant ions distributed in both the cation sites, defect fluorite structure has a better ability to tolerate radiation damage.[22]

HLW, such as uranium (U) and its isotopes, need to be properly disposed of at high concentrations due to its presence in large quantities in spent fuel, even after reprocessing.[23] Due to the multiple oxidation states and their respective health hazards, these compounds need to be carefully contained in the proper host matrix.[24] Depending on the synthesis conditions, thermal treatment, and the host matrix, U^{6+} can form UO_4^{2-}, UO_6^{6-}, and UO_2^{2+} in different molecular structures. Of these uranium ions, UO_2^{2+} is the most stable and established form of natural and spent uranium in the environment.[23] There is a large body of literature on studying the U oxidation states in pyrochlore nanoparticles such as $Gd_2Zr_2O_7$, $Nd_2Zr_2O_7$, and $La_2Zr_2O_7$.[25-27] However, the effect of high U doping concentration to the local structure, as well as the formation of different U compounds in different host matrices, has not been investigated systematically for the formation of highly stable HLW materials.

Therefore, in this work, the oxidation state of U ions and resultant molecular structures in potential HLW host matrices of $La_2Hf_2O_7$ (LHO) and $Gd_2Hf_2O_7$ (GHO) were studied to elucidate the effect of host structure (LHO with ordered pyrochlore structure *vs.* GHO with disordered fluorite structure). For this purpose, U doped LHO and GHO nanoparticles (NPs) were synthesized using a combined two-step co-precipitation and molten-salt method. XRD and Rietveld refinement was performed to identify the lattice parameters after incorporation of U in the host matrices and probe the crystal structure evolution with U doping. Next, XPS and XANES were employed to study the change in the oxidation state of U with increasing U concentration in the hosts. The characterization of the crystal structure evolution coupled with U oxidation state probing, highlights the potentiality of LHO and GHO host matrices as a new generation of stable nuclear waste forms that can provide long-life for nuclear waste storage.

2. Experimental

The synthesis process followed the combined co-precipitation and molten-salt synthesis procedure previously reported.[28] Specifically, lanthanum nitrate hexahydrate ($La(NO_3)_3•6H_2O$, 99.0%), gadolinium(III) nitrate hexahydrate ($Gd(NO_3)_3·6H_2O$, 99.9%), hafnium dichloride oxide octahydrate ($HfOCl_2•8H_2O$, 98%), and uranyl(VI) nitrate hexahydrate ($UO_2(NO_3)_2•6H_2O$, 98-102%) were used as reactants with no further purifications. For synthesizing the LHO:U NPs, a stoichiometric mixture of $La(NO_3)_3•6H_2O$, $UO_2(NO_3)_2•6H_2O$, and 5 mmol of $HfOCl_2•8H_2O$ were dissolved in 200 mL of water (Millipore, 18.2 MΩ at 25 °C) with continuous stirring. Then 200 mL of 10% ammonia solution (NH_4OH, 28-30%) was added dropwise into this solution with stirring for 2 h. The resulting precursor was then washed, vacuum filtered, and dried at 90 °C overnight. The dried precursor was mixed with sodium nitrate ($NaNO_3$, 98%) and potassium nitrate (KNO_3, 99%) with a molar ratio of 1:30:30, and ground together using a mortar and pestle into a fine powder. The powder was transferred to a crucible and annealed in a furnace at 650 °C for 6 h. The final product was washed with DI water several times and dried. Finally, a fine LHO:U powder was obtained. In this work, the U doping levels for LHO and GHO are up to 30 mol%. A similar process was followed for synthesizing the GHO:U NPs. To limit U contamination and radiation exposure, all sample preparation was performed in designated areas within the fume hood. Particulate masks were worn during handling of all U containing compounds in addition to standard personal protective equipment. All waste was collected and disposed of through the university radiation safety department.

The crystal structure of the LHO:U and GHO:U NPs was studied by performing powder X-ray Diffraction (XRD) using PANalytical X-ray diffractometer operating at 45 kV and 40 mA. The 2θ radial scan was performed using Cu Kα (λ = 1.54 Å) radiation source from 5 to 70° with a step size of 0.03°. Rietveld refinement was performed on the resultant diffraction patterns using the GSAS II software[29] for structural verification and phase quantification. Full structural refinement was achieved by performing the procedure outlined in ref[30].

The Raman spectra for the LHO:U and GHO:U NPs were collected with a Renishaw Raman spectrometer (Renishaw-2000 with 514 nm, 5 mW Ar laser or inVia Reflex Raman Spectrometer with a 532 nm, 0.05 mW laser diode). Spectra were collected with an exposure time of 0.5 s, and spectral resolution of 1 cm^{-1}. The diameter of the focused laser spot on the sample at 50x magnification was approximately 5 μm. The spectra reported here are obtained after averaging the data from three scans.

Inductively Coupled Plasma Optical Emission Spectrometer (ICP-OES) was performed using a Perkins Elmer Optima 8000 with an auto sampler. Samples for ICP-OES analysis were prepared by digesting 10 mg of the LHO:U or GHO:U NPs in a mixed HNO_3 (MiliporeSigma, 65%) and HCl (VWR BDH Chemicals, 38%) solution heated to ~90 °C. Next, the digested sample was diluted to 10 ppm using 2% HNO_3. Meanwhile, metal ion (La, Hf, Gd, U) standards (1000 ppm, ARISTR) were diluted to 5, 10, 20 ppm with 2% HNO_3 for calibration.

X-ray Photoelectron Spectroscopy (XPS) measurements of the LHO:U or GHO:U NPs were performed on a Scienta Omicron ESCA 2SR XPS system equipped with a monochromatic Al Kα ($h\nu$-1486.6 eV) X-ray source and a hemispherical analyzer with a 128-channel detector. The inherent Gaussian width of the photon source was 0.2 eV and the pressure inside the chamber was maintained at 1.5×10^{-9} Torr. The XPS spectra were calibrated to adventitious C 1*s* peak at

284.6 eV. Peak quantification was performed using Voigt function (70% Gaussian and 30% Lorentzian) in CasaXPS software[31] after subtracting the Shirley background. Soft X-Ray Absorption Spectroscopy (XAS) was used to probe the local electronic structure of the LHO:U or GHO:U NPs. O K-edge and U N-edge spectra were collected at the varied line space plane grating monochromator (VLSPGM: 0.2-1.2 keV) beamline.[32] The samples were dispersed on carbon tape and were placed inside the vacuum chamber using a load-lock. Total electron yield (TEY) detection mode with higher energy grating and 100 µm slit width was used for these low energy XAS measurements. The obtained XANES data were analyzed using Athena software.[33]

3. Results and Discussion

The LHO:U and GHO:U NPs were synthesized via the combined co-precipitation and molten salt process with equimolar La+U (or Gd+U) to Hf precursor ratio as described in the experimental section.[28] All diffraction peaks of the XRD pattern of the LHO:U NPs (Figure 1(a)) are indexed to the cubic $La_2Hf_2O_7$ phase (ICDD 037-1040, space group: *Fd-3m*),[34] indicating no impurity phases formation with up to 30 mol% U doping. The lattice parameters, calculated using the Bragg's law, are inversely proportional to the U concentration (Figure 1(c)) due to the smaller size of U ions compared with La,[35-36] confirming the incorporation of U into the LHO lattice in accordance with the Vegard's law. Similarly, the GHO:U NPs (Figure 1(b)) can also be indexed to the cubic stoichiometric $Gd_2Hf_2O_7$ phase (ICDD 24-0425, space group: *Fm-3m*) for low doping concentrations. At 30 mol% U, the diffraction peaks include a shoulder at slightly higher angles matching the non-stoichiometric $Gd_{0.44}Hf_{0.56}O_{1.78}$ phase (ICDD 04-002-0555, space group *Fm-3m*). Unlike the LHO host, the lattice parameters of the GHO:U NPs (Figure 1(d)) are relatively constant between 5.24 to 5.25 Å for all doping concentrations except for the 30 mol% U, which is much larger (5.29 Å) due to the non-stoichiometry phase. The relatively stable lattice parameter of the

GHO:U NPs with low U concentrations corresponds to the similar size of Hf and U,[36] allowing the U to occupy Hf sites in GHO hosts. It is believed that this does not occur in the LHO due to the different oxygen distribution of the two hosts. As shown in Figure 1 (c and d), the particle size of the LHO NPs, calculated based on Scherrer equation, decreases with U incorporation (0 mol% U, 14.8 nm; 5 mol% U, 14.0 nm; 30 mol% U, 5.8 nm). The undoped GHO NPs have sizes of 10.6 nm, which increases with U incorporation (5 mol%, 11.1 nm) with a slight reduction at 10 mol%, the size slightly reduces to 10.9 nm. Finally, further increasing the U concentration to 30 mol% results in particle sizes of 13.68 nm.

To further highlight the effect of U doping on the host matrices, Rietveld refinement was performed. The XRD patterns for the undoped and 30 mol% U doped samples were refined using $La_2Hf_2O_7$,[34] $Gd_2Hf_2O_7$,[37] and $Gd_{0.44}Hf_{0.56}O_{1.78}$[38] as structural models. Due to the high U concentrations, attempts were made to refine these structures along with uranium oxide (i.e. UO_2, UO_3, U_3O_8, etc.) as an initial models, but resulted in very high statistical values (R_p, $R_{wp} > 20\%$ and $\chi^2 > 10$) or unstable refinements (data not included), indicating homogeneous dopant incorporation. A summary of the crystallographic data and final refinement details are listed in Tables S1 and S2 of the Supporting Information. The fits were deemed to be good based on these parameters coupled with visual confirmation (see Figures S1 and S2). The refined LHO and GHO lattice parameters were determined to be 10.799(8) and 5.263(6) Å for the undoped and 10.745(0) and 5.312(3) Å for 30 mol% U doped crystals and are in good agreement with the calculated values. From the refined crystal structure of GHO:U (30 mol%), the amount of $Gd_2Hf_2O_7$ and $Gd_{0.44}Hf_{0.56}O_{1.78}$ (a = 5.228(9) Å) phases is estimated to be 31 and 69 wt%, respectively. The schematic drawing in Figures S1 (b and d) and S2 (b and d) illustrates that U incorporation into the La (in the case of LHO) and Hf (in the case of GHO) sites create noticeable effects on the coordination environment. In the LHO crystal, the La/U-O bond length increases from 2.24 Å to 2.33 Å, which is coupled with an even greater decrease in the Hf-O bond length (from 2.44 Å to 2.21 Å), resulting in the observed reduction in the crystal size. However, in the GHO crystal, the increasing Hf/U-O bond length (from 2.28 Å to 2.30 Å) combined with an equally increasing Gd-O bond length causes the overall crystal structure to expand, which is consistent with Figure 1(d). Based on these results, the U-O bond length in these crystals is approximated to be in the range of 2.30 to 2.33 Å, which coincides with reported values for U^{6+}-O.[39-40]

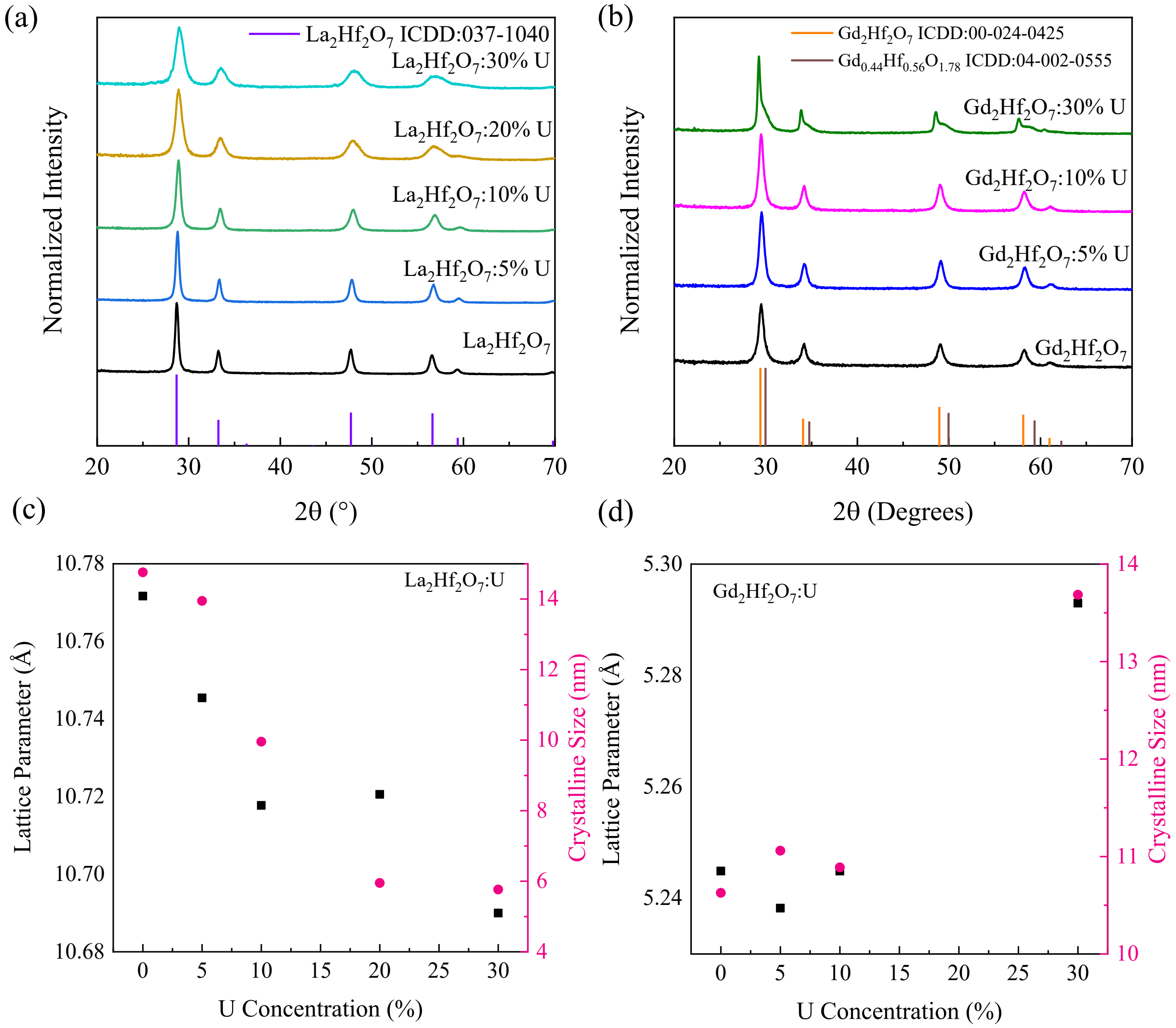

Figure 1. XRD patterns of (a) the $La_2Hf_2O_7$:U NPs (0, 5, 10, 20, 30%) with $La_2Hf_2O_7$ stoichiometry reference (ICDD 37-104) and (b) the $Gd_2Hf_2O_7$:U (0, 5, 10, 30%) with $Gd_2Hf_2O_7$ stoichiometry reference (ICDD 24-0425) and $Gd_{0.44}Hf_{0.56}O_{1.78}$ reference (ICDD 04-002-0555), showing the formation of a non-stoichiometric phase at 30 mol% U doping. (c & d) Dopant effect on lattice parameters and crystalline sizes of the $La_2Hf_2O_7$ and $Gd_2Hf_2O_7$ hosts.

ICP-OES (Table 1) was performed to quantify the stoichiometries of the LHO:U and GHO:U NPs. In the LHO:U NPs, the ratio of (La+U):Hf is not affected by the U concentration, implying the substitution of U into the La sites. Additionally, the measured concentrations match the co-precipitation solution indicating the facile incorporation at all U doping concentrations. On the other hand, the (Gd+U):Hf ratio becomes more uniform (1:0.79 to 1:0.89) with increasing U doping concentration. This response suggests that the Gd-O-Hf bonds are more difficult to form and is believed to be due to the oxygen distribution in the previously identified disordered fluorite phase. The increased Hf incorporation at the GHO:U (30 mol%) NPs is believed to be caused by the formation of the $Gd_{0.44}Hf_{0.56}O_{1.78}$ observed in the XRD pattern. These effects are believed to be due to charge compensation stemming from the U^{6+} replacing RE^{3+}/Hf^{4+} and the formation of oxygen vacancies. Overall, the two-step synthesis process[19-20, 28, 30] results in highly doped LHO:U and GHO:U crystalline NPs with unexpected phase transitions which are thought to be due to the different interactions between the ordered pyrochlore/disordered fluorite phase and the U incorporation.

Table 1. ICP data of the $La_2Hf_2O_7$:U NPs (0, 10, 20%) and the $Gd_2Hf_2O_7$:U NPs (0, 10, 30%)

	La mmol/L	Hf mmol/L	U mmol/L	Stoichiometry
$La_2Hf_2O_7$	1.20×10^{-1}	1.09×10^{-1}	0	$La_2Hf_{1.82}O_{7-\delta}$
$La_2Hf_2O_7$: 10%U	9.78×10^{-2}	9.88×10^{-2}	1.12×10^{-2}	$(La_{0.90}U_{0.10})_2Hf_{1.82}O_{7-\delta}$
$La_2Hf_2O_7$: 20%U	1.80×10^{-2}	2.02×10^{-2}	4.23×10^{-2}	$(La_{0.80}U_{0.20})_2Hf_{1.81}O_{7-\delta}$
	Gd mmol/L	Hf mmol/L	U mmol/L	
$Gd_2Hf_2O_7$	1.13×10^{-1}	8.91×10^{-2}	0	$Gd_2Hf_{1.58}O_{7-\delta}$
$Gd_2Hf_2O_7$: 10%U	1.13×10^{-1}	1.04×10^{-1}	1.11×10^{-2}	$(Gd_{0.91}U_{0.09})_2Hf_{1.67}O_{7-\delta}$
$Gd_2Hf_2O_7$: 30%U	3.42×10^{-2}	4.15×10^{-2}	1.28×10^{-2}	$(Gd_{0.73}U_{0.27})_2Hf_{1.77}O_{7-\delta}$

Raman spectroscopy was employed to further identify the change in the structure with increasing U doping concentration in LHO and GHO host. The Raman spectra for the pyrochlore LHO:U NPs has six Raman active modes, which are based on $\Gamma = A_{1g} + E_g + 4F_{2g}$ according to group theoretical analysis[41] (Figure S3(a)).[18] Meanwhile, additional peaks at ~717 cm^{-1} and ~765 cm^{-1} are observed with 5 mol% U doping due to the U-O stretching vibrations in typical U^{6+} structure (Orthorhombic α-UO$_3$).[42-43] These vibrations red shift to 700 cm^{-1} and merge with increasing U doping concentration, indicative of elongated U-O bonds. Additionally, the pyrochlore peaks are broadened and are still present at the highest U concentration (Figure S3(b)), suggesting a transformation to the disordered fluorite structure. Conversely, since O^{2-} ions are randomly distributed around both cation sites, only one Raman active mode (F$_{2g}$) is expected for the disordered fluorite GHO:U NPs (Figure S3(c)).[44] This peak is not present at 30 mol% U due to the formation of the defect phase. Similar to the LHO:U NPs, the peak at ~716 cm^{-1} and the shoulder peak at ~771 cm^{-1} red shift with increasing U incorporation. This red shift is correlated to an extension of the RE-O bonds, and agrees with the larger lattice parameter and elongated La/Gd-O bond observed in the Rietveld refinement at 30 mol% U. Overall, the combination of Rietveld refinement and Raman results confirm the formation of U^{6+}-O structures in both host matrices. Furthermore, the GHO:U NPs undergo a phase transformation as seen in the XRD patterns (Figure 1), while the LHO:U NPs have a relatively stable pyrochlore/disordered fluorite structure even at high U concentrations.

XANES and XPS were performed to confirm the oxidation state of U and understand the respective cluster formation in the LHO:U and GHO:U NPs. Figure 2 shows the O K-edge XANES of LHO, GHO, and UO$_2$ and U$_3$O$_8$ standards. In LHO (Figure 2(a)), a pre-edge peak at 530.0 eV appears at 5 mol% doping and increases proportionally with increasing U doping concentration. This is ascribed to a U $5f$ – O $2p$ hybridized band, which can be attributed to the pre-edges of either

U_3O_8 or UO_2 standards.[45] The hybridized O 2*p* - La 5*d*/Hf 5*d* t_{2g} orbitals signature at 533.1 eV (#) has two distinct peaks for the undoped LHO which has been attributed to a distorted La/Hf-O octahedra.[46] After introducing U into the LHO NPs, the peaks merge into a broadened single peak due to the overlap with the hybridized O 2*p*/U 5*f* state and also distortion in the crystal lattice.[47] Next, the appearance of the ascribed transition of O 1*s* to a hybridized O 2*p*/U 6*d* t_{2g} orbital at 536.7 eV coincides with the U^{6+} absorption in U_3O_8 standard.[45, 48] The additional peaks observed are not affected by the U inclusion: O 2*p* hybridized peaks at 538 eV (Hf 5*d* e_g/La 6*p* states[49]), and the peaks at 542.2-544 eV (Hf 6*sp* states[49]). For comparison, the XANES spectra of the GHO:U NPs are shown in Figure 2(b). Interestingly, only minor changes were observed with the peaks at 530.0 eV and 536.7 eV (#), which is regarded as the consequence of the formation of U^{6+} and defects.[50] This can also explain the equivalence of the cation sites in disordered fluorite structure, so that the incorporation of U can equally occupy any

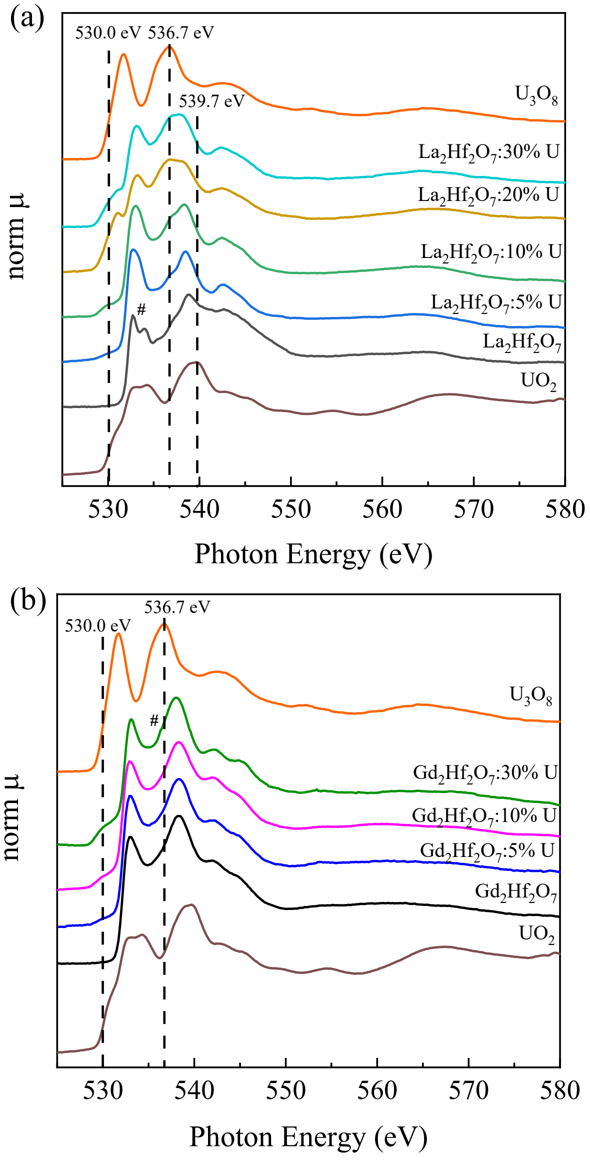

Figure 2. XANES O K edge of (a) $La_2Hf_2O_7$: U (0, 5, 10, 20, 30%) and (b) $Gd_2Hf_2O_7$: U (0, 5, 10, 30%) comparing with UO_2, and U_3O_8 standards.

cation site without changing the overall local structure. Furthermore, the U N-edge was probed to directly quantify the U oxidation states (Figure S4). In this case, a slight blue shift[51] was observed in the N edges suggesting a slightly more oxidized state while doping of the GHO resulted in no noticeable change in oxidation state. Ultimately, the O K-edge XANES spectra of the LHO and GHO hosts show the presence of two different U^{6+} molecular structures which are responsible for the phase changes seen in the previous XRD and Raman results.

Next, XPS was performed to study the change in the concentration of oxygen vacancies (O_v) and local coordination environment of other cations in the host matrix. Figures 3 and 4 show the O 1*s*, Hf 4*p*/U 4*f*, Hf 4*f*, Gd 4*d*, and La 3*d* detailed XPS scans of the LHO:U and GHO:U NPs, respectively. Initially, the LHO O 1*s* spectra (Figure 3(a)) exhibits an increase in O_v with U concentration up to 20%, indicating the

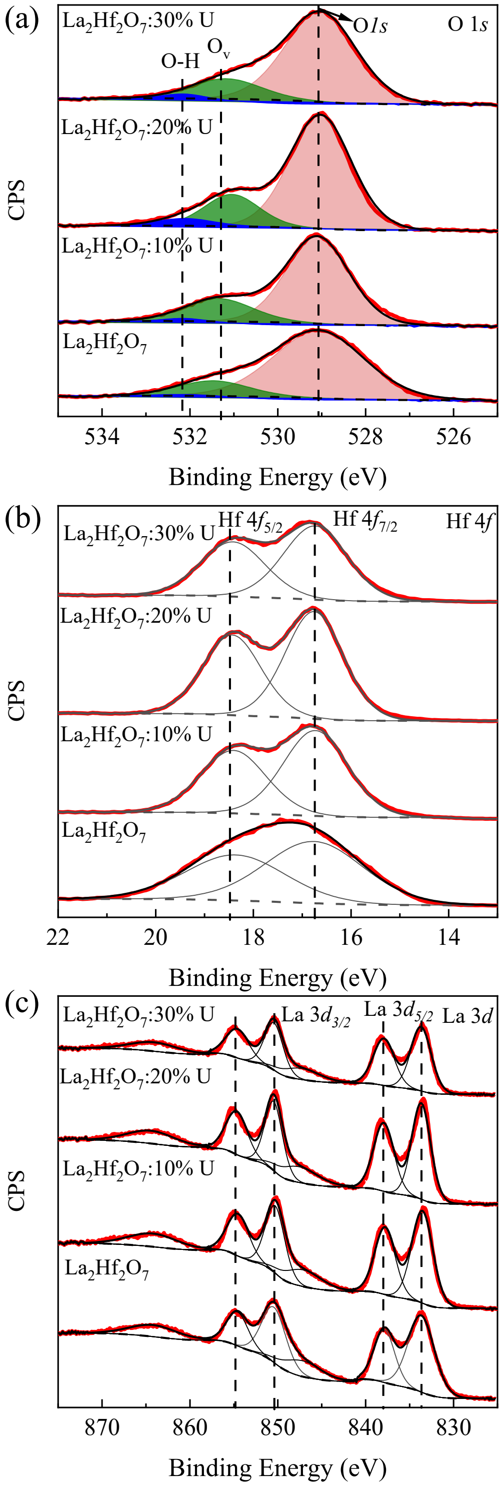

Figure 3. (a) O 1*s*, (b) Hf 4*f*, and (c) La 3*d* XPS spectra of the $La_2Hf_2O_7$:U NPs (0, 5, 10, 30%).

formation of defected U sites which are responsible for the Raman phase transformation. The O_V concentration then decreases as the U concentration further increases to 30%. This is attributed to a change from the UO_6^{6-} to the UO_2^{2+} structure according to charge compensation. The Hf 4*p*/U 4*f* spectra (Figure S5(a)) show the range of 375-460 eV with the overlap of Hf $4p_{3/2}$ and U $4f_{7/2}$. The peaks Hf $4p_{3/2}$ (380.7 eV) and Hf $4p_{1/2}$ (437.5 eV) are identified by undoped LHO reference. The peak positions of U $4f_{7/2}$ and U $4f_{5/2}$ are observed as 380.7 eV and 391.5 eV, respectively, and are similar to those expected for the U^{5+}/U^{6+} energies seen in U_3O_8.[52] In light of this, the uranium is not expected to be reduced during the synthesis, maintaining its U^{6+} oxidation state. In Hf 4*f* and La 3*d* spectra (Figure 3(b, c)), no significant changes were observed at different U doping

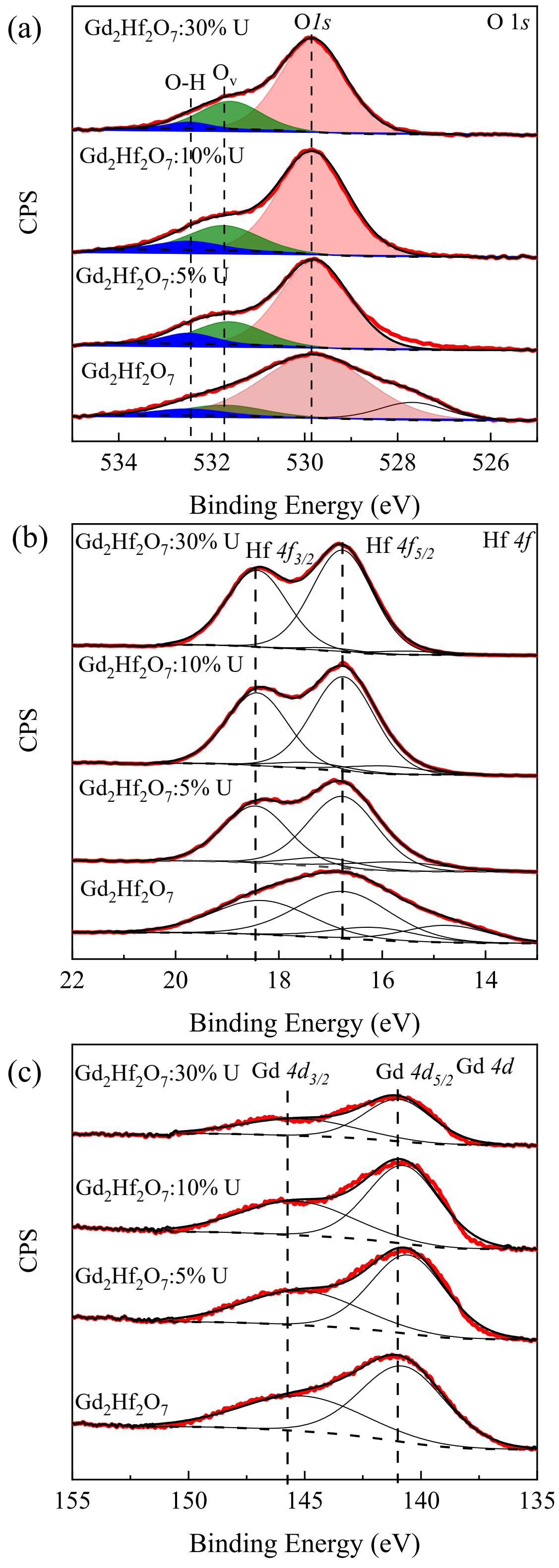

Figure 4. (a) O 1*s*, (b) Hf 4*f*, and (c) Gd *4d* XPS spectra of the $Gd_2Hf_2O_7$:U NPs (0, 5, 10, 30%).

concentrations, showing that the local structures of these two sites are not affected by the introduction of U. As a result, the oxygen vacancy concentration in this LHO:U matrix is influenced by the formation of different forms of U^{6+} (UO_6^{6-} and UO_2^{2+}) at high doping concentrations.

In the case of the GHO host, the O_v concentration increases upon incorporation of U and remains relatively stable despite the growing U concentration (Figure 4(a)), which is in accordance with the XANES results. The Hf 4*p* and U 4*f* spectra (Figure S5(b)) of the GHO:U NPs show the same position of Hf $4p_{3/2}$ (380.7 eV) and Hf $4p_{1/2}$ (437.5 eV) compared to the undoped GHO reference. Alternatively, the positions of U $4f_{7/2}$ and U $4f_{5/2}$ peaks red shift to 380.3 eV and 391.1 eV, respectively. These positions are at lower binding energy than that of U_3O_8,[52] which shows that U ions have a lower average oxidation state in the GHO host than the LHO host. In the Hf 4*f* XPS spectra (Figure 4(b)), the peaks at 14.8 eV and 16.3 eV are observed in undoped GHO host and are related to a HfO_{2-x} species, indicating the formation of oxygen vacancies surrounding the Hf sites.[20, 53] After introducing U into the host matrix, these peaks disappear suggesting a more uniform Hf binding environment throughout the crystal. Contrary to the Hf 4*f* XPS spectra, the Gd 4*d* spectra do not change with U incorporation (Figure 4(c)) because Gd^{3+} cannot be further oxidized. Therefore, the increasing U doping in the GHO host matrix directly affects the local environment around the Hf sites. Meanwhile, the U doping does not significantly affect the overall oxygen vacancy concentration of the GHO:U NPs. This result agrees with the conclusion from XANES that the local structure of GHO remains stable with the incorporation of U.

The combined XANES and XPS results all indicate that U is stable as +6 oxidation state in the LHO:U and GHO:U NPs. By increasing the U doping, a transformation between UO_6^{6-} (LHO:20%U) or UO_2^{2+} (LHO:30%U) occurs in the LHO host which reduces oxygen vacancy concentration. In the GHO host, the UO_6^{6-} type polymorph is stable at all investigated concentrations, driving the formation of a new defect phase at higher concentrations.[13, 54] Moreover, the Rietveld refinement confirms that the presence of O_v in both host matrices distorts the octahedral coordination, which contributes to the calculated U^{6+}-O bond length (2.30 - 2.33 Å) agreeing with the reported literature value (~2.11 ± 0.22 Å).[39-40] This U^{6+}-O phenomena is seen in other $RE_2Hf_2O_7$ compounds and is attributed to the structure of the host lattice, and their associated oxygen defect distribution, exhibiting U^{6+} luminescent signatures.[13] Based on these results, it is possible to control the U^{6+}-O group structure in complex oxides by controlling the initial oxygen vacancy position and has important implications in the generation and storage of HLW without having to worry about adverse environmental impacts.

4. Conclusion

In summary, LHO:U and GHO:U NPs were synthesized using a combined co-precipitation and molten-salt synthesis method. XRD and Rietveld refinement results show that the LHO:U and GHO:U NPs formed crystalline phases even at high U doping level (30% in this study). The lattice parameter slightly decreases with increasing U doping due to the formation of UO_x ion group with different sizes compared with La^{3+} and Gd^{3+}. Raman suggested a transformation from pyrochlore to disordered fluorite structure with increasing U concentration in the LHO host. Meanwhile, Raman and XANES spectra show that U exists as U^{6+} oxidation state in both LHO and GHO host. A transformation from the UO_6^{6-} to the UO_2^{2+} structure occurs in the LHO host as confirmed with the observed changes of the lattice parameters, x-ray absorption, and oxygen vacancy O_v concentration in the LHO:U NPs. Alternatively, UO_6^{6-} structure was formed and no U transformation was observed in the GHO:U NPs, instead, a non-stoichiometric defect phase appears and is attributed to the disordered O_v distribution in the disordered fluorite GHO host. The structure of the U^{6+}-O cluster changes with increasing U concentration in the ordered pyrochlore structured LHO:U NPs, driving the transformation into the disordered fluorite phase, but remains stable in the defect fluorite structured GHO:U NPs. Overall, this LHO:U transformation allows for high U storage while also resulting in a more radiation tolerant crystal structure. Based on this study, the stability of U^{6+}-O cluster is determined by the original O_v position in the host matrices of rare-earth based $A_2B_2O_7$ compounds, which leads to a better understanding of structure-property correlation at microscopic level and the dopant-host material relationship, and can be employed to the design of HLW host materials.

ASSOCIATED CONTENT

Supporting Information.

The Supporting Information is available free of charge on the XXX website at DOI: Rietveld refinement and refined crystallographic/ structural parameters from GSAS II, Raman spectra, XANES U N-edge and XPS Hf 4*p*/U 4*f*.

Corresponding Authors

*Email: jamesdorman@lsu.edu; ymao17@iit.edu

Author Contributions

Y.W completed the XRD, Raman, XANES, XPS analysis of the LHO:U and GHO:U NPs. P.D. assisted in the XPS and XANES measurements and analysis. T.O. performed the XRD measurement and Rietveld refinement. S.G. assisted in the Raman analysis. O.K. has performed the XANES measurements and assisted in the XANES analysis. Y.M. and J.A.D. composed the study and designed the experiments. Y.W. and J.A.D. initiated the writing of the manuscript. All authors contributed to the manuscript.

ACKNOWLEDGMENT

J.A.D and Y.W would like to acknowledge support from the National Science Foundation grant CHE-1709902. Y.M. would like to thank the financial support by the National Science Foundation under CHE (award #1710160). P.D. is thankful to the Graduate School of Louisiana State University for the Dissertation Year Fellowship. T.O. acknowledges the fellowship support from the Louisiana College of Engineering and CHE-1709902 for supplies. S.K.G thanks the United States-India Education Foundation (USIEF) and the Institute of International Education (IIE) for the Fulbright Nehru Postdoctoral Fellowship (Award# 2268/FNPDR/2017). The authors also acknowledge the support of the staff of the CAMD synchrotron light source. The authors would also like to thank Andrew Miskowiec, Sarah Finkeldei (currently at University of California, Irvine), and Tyler Spano from Oak Ridge National Labs for suppling the uranium oxide powder standards. We also thank Behnam Safavinia for assisting ICP-OES measurements and M. Abdou for assistance with sample preparation.

REFERENCES

1. Vienna, J. D.; Ryan, J. V.; Gin, S.; Inagaki, Y., Current Understanding and Remaining Challenges in Modeling Long‐Term Degradation of Borosilicate Nuclear Waste Glasses. *Int J Appl Glass Sci* **2013**, *4*, 283-294.
2. Mendel, J. E., High-Level Waste Glass. *Nuclear Technology* **1977**, *32*, 72-87.
3. Hench, L.; Clark, D.; Campbell, J., High Level Waste Immobilization Forms. *Nucl Chem Waste Man* **1984**, *5*, 149-173.

4. Grambow, B.; Lutze, W., Chemical Stability of a Phosphate Glass under Hydrothermal Conditions. In *Scientific Basis for Nuclear Waste Management*, Springer: 1980; pp 109-116.

5. McCarthy, G. J.; Davidson, M. T., Ceramic Nuclear Waste Forms. I. Crystal Chemistry and Phase Formation. *Am. Ceram. Soc. Bull.* **1975**, *54*, 782-786.

6. Ringwood, A. E.; Kesson, S. E.; Ware, N. G.; Hibberson, W.; Major, A., Immobilisation of High Level Nuclear Reactor Wastes in Synroc. *Nature* **1979**, *278*, 219-223.

7. Moore, J.; Rogers, G.; Katz, S.; Morgan, M.; Newman, E., Fuetap Concretes-Tailored Autoclaved Concretes for the Fixation of Radioactive Wastes. *Waste Manage* **1981**, *81*, 267.

8. McCarthy, G.; White, W.; Roy, R.; Scheetz, B.; Komarneni, S.; Smith, D.; Roy, D., Interactions between Nuclear Waste and Surrounding Rock. *Nature* **1978**, *273*, 216-217.

9. Mandal, B.; Pandey, M.; Tyagi, A., $Gd_2Zr_2O_7$ Pyrochlore: Potential Host Matrix for Some Constituents of Thoria Based Reactor's Waste. *J. Nucl. Mater* **2010**, *406*, 238-243.

10. Gregg, D. J.; Zhang, Y.; Zhang, Z.; Karatchevtseva, I.; Blackford, M. G.; Triani, G.; Lumpkin, G. R.; Vance, E. R., Crystal Chemistry and Structures of Uranium-Doped Gadolinium Zirconates. *J. Nucl. Mater* **2013**, *438*, 144-153.

11. Sickafus, K.; Minervini, L.; Grimes, R.; Valdez, J.; Ishimaru, M.; Li, F.; McClellan, K.; Hartmann, T., Radiation Tolerance of Complex Oxides. *Science* **2000**, *289*, 748-751.

12. Wilde, P.; Catlow, C., Defects and Diffusion in Pyrochlore Structured Oxides. *Solid State Ion.* **1998**, *112*, 173-183.

13. Abdou, M.; Gupta, S. K.; Zuniga, J. P.; Mao, Y., Insight into the Effect of A-Site Cations on Structural and Optical Properties of $RE_2Hf_2O_7$: U Nanoparticles. *J. Lumin* **2019**, *210*, 425-434.

14. Gu, S.; Zhang, S.; Xue, B.; Yan, J.; Li, W.; Zhang, L., Phase Variation and Thermophysical Properties of $La_2Hf_2O_7$ with Alumina Addition. *J Eur Ceram Soc* **2018**, *38*, 1938-1945.

15. Vorozhtcov, V. A.; Stolyarova, V. L.; Lopatin, S. I.; Simonenko, E. P.; Simonenko, N. P.; Sakharov, K. A.; Sevastyanov, V. G.; Kuznetsov, N. T., Vaporization and Thermodynamic Properties of Lanthanum Hafnate. *J Alloy Compd* **2018**, *735*, 2348-2355.

16. Turner, K. M.; Rittman, D. R.; Heymach, R. A.; Tracy, C. L.; Turner, M. L.; Fuentes, A. F.; Mao, W. L.; Ewing, R. C., Pressure-Induced Structural Modifications of Rare-Earth Hafnate Pyrochlore. *J. Condens. Matter Phys.* **2017**, *29*, 255401.

17. Sun, M.; Huang, B., Comparison and Correlation of Structural Disorder Caused by Anion Frenkel in Affecting Ion Conduction of La 2 Hf 2 O 7 and La 2 Mo 2 O 9 as High Performance Electrolytes in Sofcs. *MRS Adv.* **2017**, *2*, 3317-3322.

18. Pokhrel, M.; Wahid, K.; Mao, Y., Systematic Studies on $RE_2Hf_2O_7$: 5% Eu^{3+} (Re= Y, La, Pr, Gd, Er, and Lu) Nanoparticles: Effects of the A-Site RE^{3+} Cation and Calcination on Structure and Photoluminescence. *J Phys Chem C* **2016**, *120*, 14828-14839.

19. Wang, Y.; Darapaneni, P.; Kizilkaya, O.; Dorman, J. A., Role of Ce in Manipulating the Photoluminescence of Tb Doped $Y_2Zr_2O_7$. *Inorg. Chem* **2020**, *59*, 2358-2366.

20. Safavinia, B.; Wang, Y.; Jiang, C.; Roman, C.; Darapaneni, P.; Larriviere, J.; Cullen, D. A.; Dooley, K. M.; Dorman, J. A., Enhancing $Ce_xZr_{1-x}O_2$ Activity for Methane Dry Reforming Using Subsurface Ni Dopants. *ACS Catal* **2020**, *10*, 4070-4079.

21. Bhattar, S.; Krishnakumar, A.; Kanitkar, S.; Abedin, A.; Shekhawat, D.; Haynes, D. J.; Spivey, J. J., 110th Anniversary: Dry Reforming of Methane over Ni- and Sr-Substituted Lanthanum Zirconate Pyrochlore Catalysts: Effect of Ni Loading. *Ind. Eng. Chem. Res.* **2019**, *58*, 19386-19396.

22. Sickafus, K. E.; Grimes, R. W.; Valdez, J. A.; Cleave, A.; Tang, M.; Ishimaru, M.; Corish, S. M.; Stanek, C. R.; Uberuaga, B. P., Radiation-Induced Amorphization Resistance and Radiation Tolerance in Structurally Related Oxides. *Nat. Mater.* **2007**, *6*, 217-223.

23. Gupta, S. K.; Reghukumar, C.; Pathak, N.; Sudarshan, K.; Tyagi, D.; Mohapatra, M.; Pujari, P.; Kadam, R., Speciation of Uranium and Doping Induced Defects in $Gd_{1.98}U_{0.02}Zr_2O_7$: Photoluminescence, X-Ray Photoelectron and Positron Annihilation Lifetime Spectroscopy. *Chem. Phys. Lett* **2017**, *669*, 245-250.

24. Natrajan, L. S., Developments in the Photophysics and Photochemistry of Actinide Ions and Their Coordination Compounds. *Coord. Chem. Rev.* **2012**, *256*, 1583-1603.

25. Govindan Kutty, K. V.; Asuvathraman, R.; Raja Madhavan, R.; Jena, H., Actinide Immobilization in Crystalline Matrix: A Study of Uranium Incorporation in Gadolinium Zirconate. *J. Phys. Chem. Solids* **2005**, *66*, 596-601.

26. Shu, X.; Lu, X.; Fan, L.; Yang, R.; Ding, Y.; Pan, S.; Zhou, P.; Wu, Y., Design and Fabrication of $Gd_2Zr_2O_7$-Based Waste Forms for U_3O_8 Immobilization in High Capacity. *J. Mater. Sci* **2016**, *51*, 5281-5289.

27. Zhang, F. X.; Lang, M.; Tracy, C.; Ewing, R. C.; Gregg, D. J.; Lumpkin, G. R., Incorporation of Uranium in Pyrochlore Oxides and Pressure-Induced Phase Transitions. *J. Solid State Chem.* **2014**, *219*, 49-54.

28. Abdou, M.; Gupta, S. K.; Zuniga, J. P.; Mao, Y., On Structure and Phase Transformation of Uranium Doped $La_2Hf_2O_7$ Nanoparticles as an Efficient Nuclear Waste Host. *Mater. Chem. Front* **2018**, *2*, 2201-2211.

29. A. C. Larson and R. B. Von Dreele, General Structure Analysis System (GSAS), report LAUR 86-748, Los Alamos National Laboratory, NM, **1994**.

30. Ofoegbuna, T.; Darapaneni, P.; Sahu, S.; Plaisance, C.; Dorman, J. A., Stabilizing the B-Site Oxidation State in ABO_3 Perovskite Nanoparticles. *Nanoscale* **2019**, *11*, 14303-14311.

31. Fairley, N., *Casaxps Manual 2.3. 15: Casaxpx Processing Software for Xps Spectra*; Casa Software Limited, 2009.

32. Morikawa, E.; Ono, M.; Kodukula, S.; Bordelon, A.; Scott, J.; Garber, J.; Perkins, R. In *Infrared Microspectroscopy Beamline at Camd*, AIP Conference Proceedings, AIP: 2004; pp 364-367.

33. Ravel, B.; Newville, M., Athena, Artemis, Hephaestus: Data Analysis for X-Ray Absorption Spectroscopy Using Ifeffit. *J. Synchrotron Radiat.* **2005**, *12*, 537-541.

34. Kaichev, V.; Smirnova, T.; Yakovkina, L.; Ivanova, E.; Zamoryanskaya, M.; Saraev, A.; Pustovarov, V.; Perevalov, T.; Gritsenko, V., Structure, Chemistry and Luminescence Properties of Dielectric $La_xHf_{1-x}O_y$ Films. *Mater Chem Phys* **2016**, *175*, 200-205.

35. Kim, D. J., Lattice Parameters, Ionic Conductivities, and Solubility Limits in Fluorite‐Structure MO_2 Oxide [M= Hf^{4+}, Zr^{4+}, Ce^{4+}, Th^{4+}, U^{4+}] Solid Solutions. *J Am Ceram Soc* **1989**, *72*, 1415-1421.

36. Ahrens, L. H., The Use of Ionization Potentials Part 1. Ionic Radii of the Elements. *Geochim. Cosmochim. Acta* **1952**, *2*, 155-169.

37. McIlvried, M., Penn State University, University Park, Pennsylvania, USA. *ICDD Grant-in-Aid* **1972**.

38. Shevchenko, A.; Lopato, L.; Nazarenko, L., Systems of HfO_2 with Oxides of Samarium, Gadolinium, Terbium, and Dysprosium at High Temperatures. *Inorg. Mater.* **1984**, *20*, 1615.

39. Gagné, O. C., Bond-Length Distributions for Ions Bonded to Oxygen: Results for the Lanthanides and Actinides and Discussion of the F-Block Contraction. *Acta Crystallogr B* **2018**, *74*, 49-62.
40. Burns, P. C., U^{6+} Minerals and Inorganic Compounds: Insights into an Expanded Structural Hierarchy of Crystal Structures. *Can Mineral* **2005**, *43*, 1839-1894.
41. Garg, N.; Pandey, K.; Murli, C.; Shanavas, K.; Mandal, B. P.; Tyagi, A.; Sharma, S. M., Decomposition of Lanthanum Hafnate at High Pressures. *Phys. Rev. B Condens. Matter* **2008**, *77*, 214105.
42. Palacios, M. L.; Taylor, S. H., Characterization of Uranium Oxides Using in Situ Micro-Raman Spectroscopy. *Appl. Spectrosc.* **2000**, *54*, 1372-1378.
43. Stefaniak, E. A.; Alsecz, A.; Sajó, I. E.; Worobiec, A.; Máthé, Z.; Török, S.; Van Grieken, R., Recognition of Uranium Oxides in Soil Particulate Matter by Means of M-Raman Spectrometry. *J. Nucl. Mater.* **2008**, *381*, 278-283.
44. Gupta, S. K.; Abdou, M.; Ghosh, P. S.; Zuniga, J. P.; Mao, Y., Thermally Induced Disorder–Order Phase Transition of $Gd_2Hf_2O_7$: Eu^{3+} Nanoparticles and Its Implication on Photo- and Radioluminescence. *ACS omega* **2019**, *4*, 2779-2791.
45. Jollet, F.; Petit, T.; Gota, S.; Thromat, N.; Gautier-Soyer, M.; Pasturel, A., The Electronic Structure of Uranium Dioxide: An Oxygen K-Edge X-Ray Absorption Study. *J. Condens. Matter Phys.* **1997**, *9*, 9393.
46. Wu, Z.; Benfatto, M.; Pedio, M.; Cimino, R.; Mobilio, S.; Barman, S.; Maiti, K.; Sarma, D., Theoretical Analysis of X-Ray-Absorption near-Edge Fine Structure at the O and Metal K Edges of $LaFeO_3$ and $LaCOO_3$. *Phys. Rev. B Condens. Matter* **1997**, *56*, 2228.
47. Wen, X.-D.; Löble, M. W.; Batista, E. R.; Bauer, E.; Boland, K. S.; Burrell, A. K.; Conradson, S. D.; Daly, S. R.; Kozimor, S. A.; Minasian, S. G., Electronic Structure and O K-Edge XAS Spectroscopy of U_3O_8. *J Electron Spectrosc* **2014**, *194*, 81-87.
48. Magnuson, M.; Butorin, S. M.; Werme, L.; Nordgren, J.; Ivanov, K. E.; Guo, J.-H.; Shuh, D. K., Uranium Oxides Investigated by X-Ray Absorption and Emission Spectroscopies. *Appl Surf Sci* **2006**, *252*, 5615-5618.
49. Blanchard, P. E.; Liu, S.; Kennedy, B. J.; Ling, C. D.; Avdeev, M.; Aitken, J. B.; Cowie, B. C.; Tadich, A., Investigating the Local Structure of Lanthanoid Hafnates $Ln_2Hf_2O_7$ Via Diffraction and Spectroscopy. *J Phys Chem C* **2013**, *117*, 2266-2273.
50. Sharma, A.; Varshney, M.; Shin, H.-J.; Chae, K.; Won, S. O., XANES, EXAFS and Photoluminescence Investigations on the Amorphous Eu: HfO_2. *Spectrochim. Acta A* **2017**, *173*, 549-555.
51. Darapaneni, P.; Kizilkaya, O.; Wang, Z.; Dorman, J. A., Weak Field Tuning of Transition-Metal Dopant Hybridization in Solid Hosts. *J Phys Chem C* **2018**, *122*, 22699-22708.
52. Allen, G. C.; Crofts, J. A.; Curtis, M. T.; Tucker, P. M.; Chadwick, D.; Hampson, P. J., X-Ray Photoelectron Spectroscopy of Some Uranium Oxide Phases. *Dalton Trans.* **1974**, 1296-1301.
53. Oh, I.-K.; Park, B.-E.; Seo, S.; Yeo, B. C.; Tanskanen, J.; Kim, W.-H.; Kim, H., Comparative Study of the Growth Characteristics and Electrical Properties of Atomic-Layer-Deposited HfO_2 Films Obtained from Metal Halide and Amide Precursors. *J Mater Chem C* **2018**, *6*, 7367-7376.
54. Darapaneni, P.; Moura, N. S.; Harry, D.; Cullen, D. A.; Dooley, K. M.; Dorman, J. A., Effect of Moisture on Dopant Segregation in Solid Hosts. *J Phys Chem C* **2019**, *123*, 12234-12241.

Table of Content